Carbon 123 (2017) 302–306

Contents lists available at ScienceDirect

Carbon

journal homepage: www.elsevier.com/locate/carbon

Raman spectra of twisted CVD bilayer graphene

Pankaj Ramnani [a, 1], Mahesh R. Neupane [b, c, 1], Supeng Ge [d], Alexander A. Balandin [b, e], Roger K. Lake [b, e, *], Ashok Mulchandani [a, e, **]

[a] Department of Chemical and Environmental Engineering, University of California, Riverside, CA 92521, USA
[b] Department of Electrical and Computer Engineering, University of California, Riverside, CA 92521, USA
[c] U.S. Army Research Laboratory, RDRL-SER-E, Adelphi, MD 20783, USA
[d] Department of Physics and Astronomy, University of California, Riverside, CA 92521, USA
[e] Materials Science and Engineering Program, University of California, Riverside, CA 92521, USA

ARTICLE INFO

Article history:
Received 21 March 2017
Received in revised form
18 July 2017
Accepted 19 July 2017
Available online 21 July 2017

ABSTRACT

The Raman spectra of large-size, single-crystal, twisted bilayer graphene (tBLG) grains grown by chemical vapor deposition (CVD) are measured as a function of the rotation angle. The rotation angle between the graphene layers is determined using a combination of transmission electron microscopy (TEM) and selected area electron diffraction (SAED). The 2D and G peaks follow the same trends as found previously. The low-frequency peaks (<200 cm^{-1}) are compared to the Γ-point modes calculated from large scale molecular dynamics simulations. In this low frequency range, the ZO′ mode and new Γ-point frequencies are observed at angles far from the resonant angle of 12°. The twist-angle dependence of the new modes is not a monotonic function of twist angle or supercell size, and this non-monotonic behavior is consistent with the zone-folded modes determined from the numerical calculations.

Published by Elsevier Ltd.

1. Introduction

Graphene is a single atom thick two-dimensional honeycomb lattice made of sp2-hybridized carbon atoms at the hexagon vertices [1]. Owing to its higher thermal conductivity [2], superior mechanical properties [3], and exceptional charge carrier mobility [4], graphene has been explored for a wide range of applications such as thermal heat spreader [5], photovoltaics [6], ultrahigh frequency electronic devices [7], etc.

When two graphene layers are stacked, either mechanically or via epitaxial growth, the resulting electrical, vibrational, thermal and optical properties depend on the relative twist angle between the layers [8]. The misoriented stacking of the layers results in low energy phonon modes which are not present in graphene and AB-stacked bilayer graphene (BLG). Such a bilayer graphene system where the two atomic planes are rotated relative to each other is often referred to as turbostatic, misoriented, or twisted bilayer graphene (tBLG). In AB-stacked bilayer graphene, the two graphene layers are such that the A-triangular sub-lattice of the top (bottom) layer lies exactly on top of the B-sub-lattice of bottom (top) layer. When one layer of graphene is rotated with respect to the other, they form a Moiré pattern, the periodicity of which represents a new structural length scale of the system [9–12].

The electrical and phonon properties of oriented bilayer graphene, typically AB-BLG have been extensively studied both experimentally [13–15] and theoretically [16,17]. The electronic structure of AB-stacked bilayer graphene consists of quadratic dispersion with two parallel parabolic conduction bands situated above another two parallel parabolic valence bands with zero bandgap [13]. For tBLG with twist angles beyond a few degrees, the low-energy states in each layer electronically decouple, and the low-energy dispersion becomes linear although with reduced velocity for angles below 10° [10,12,18–21]. In an experimental study it was found that tBLG had lower thermal conductivity as compared to AB-BLG and SLG [22]. This suggests that, unlike electrons, phonons which are the primary heat carriers, do not propagate in tBLG as in two independent SLG planes, and there is a finite degree of van der Waals interaction between the atomic planes of tBLG [22].

Raman spectroscopy has been the primary experimental tool for analyzing the vibrational properties of graphene-based systems

* Corresponding author. Department of Chemical and Environmental Engineering, University of California, Riverside, CA 92521, USA.
** Corresponding author. Department of Electrical and Computer Engineering, University of California, Riverside, CA 92521, USA.
E-mail addresses: ralake@ece.ucr.edu (R.K. Lake), adani@engr.ucr.edu (A. Mulchandani).
[1] Authors P.R and M.R.N contributed equally to this work.

http://dx.doi.org/10.1016/j.carbon.2017.07.064
0008-6223/Published by Elsevier Ltd.

such as AB-BLG and tBLG [23–28]. The angle dependence of the G-band was dominated by the resonant enhancement that occurs at the critical angle θ_c when the incident laser energy is equal to the gap between the electron and hole van-Hove singularities [24,25]. Trends in the position, width, and intensity of the 2D peaks as a function of twist angle were well described by the angle dependence of the electronic structure and the van-Hove singularities assuming the vibrational spectrum remained that of single layer graphene [25,29]. The D-peak served primarily as an indicator of the quality of the sample [25]. New low energy modes ~90 cm^{-1} were observed when the twist angle was near the critical angle for resonant enhancement of the G band [26].

Theoretical studies of the phonon dispersion have been carried out using density functional theory (DFT) [30,31], continuum models [32], and atomistic force constant models [33,34]. Owing to the smaller primitive unit cells of the SLG and AB-BLG (2 and 4 atoms respectively), DFT-based methods have been frequently used for the studies of the vibrational properties of SLG and AB-BLG. However, in the tBLG system, the primitive cell size increases exponentially from 28 atoms to thousands of atoms depending on the twist angle, which makes the DFT-based methods difficult. Recent modeling [33] of the vibrational frequencies of tBLG reproduced the high energy vibrational modes from experiments for the twist angles $\geq 7^\circ$. There have been two different studies of the low energy breathing mode using Born von Karman and Lennard Jones potentials [33,34]. The first study [33] found a decrease in the energy of ~6 cm^{-1} as the angle increased from 0 to 7.3° and then the frequency slightly increased by 0.4 cm^{-1} as the angle increased to 21.8°. Modeling of the low energy breathing mode in a circular geometry [34] with the atoms pinned at the perimeter showed an increase in the frequency of ~10 cm^{-1} as the twist angle increased from 0° to 8°. Since both the methods are based on the force-constants extracted from the DFT and only include local C-C interactions while excluding the effect of temperature induced anharmonicity during calculations, the established qualitative agreement between vibrational spectra calculated at 0 K to the experimental Raman data obtained at 300 K might be coincidental. In addition, phonon modes including low-frequency modes exhibit linear dependency in the temperature [35]. Hence, a method that can simulate larger sample, considers long-range C-C interactions, and includes temperature-dependent anharmonicity during lattice dynamics is essential for the study of low frequency modes in the tBLG systems. In this work, we present a systematic study of synthesis of tBLG using chemical vapor deposition (CVD) and characterization of twist angle using transmission electron microscopy (TEM) and Raman spectroscopy. Briefly, large sized single crystal tBLG with random orientations were grown directly on a Cu foil using ambient pressure chemical vapor deposition (AP-CVD) [36]. The nucleating density of graphene grains and growth kinetics were controlled so as to obtain micron-sized hexagonal single crystals of tBLG with twist angles covering the entire range of rotational angles. The tBLG samples were then transferred onto TEM grids using a direct (polymer free) transfer method to avoid polymer contamination. Additionally, having the graphene grains suspended over the holes of a TEM grid is necessary to avoid any interaction of the sample with the substrate that could lead to possible dampening of the Raman modes [37]. The graphene growth and transfer procedure are discussed in detail in Supplementary Information. To avoid introducing defects into the sample, the Raman characterization was performed first followed by TEM characterization [25]. The relative twist angle between the graphene bilayers for each tBLG grain was determined using selected area electron diffraction (SAED) patterns obtained using TEM. The quality and crystalline nature of the tBLG samples was further validated by comparing the twist angle dependent Raman signature (G and 2D peak) to the ones reported in literature [25,26]. Finally, we look into the details of the low frequency ZO' (or ZA) modes, which correspond to inter-layer breathing modes, and new modes that are observed in the frequency range of 90–200 cm^{-1}. We compared the frequency of the experimentally observed low frequency modes with the theoretical frequencies calculated using large scale molecular dynamics (MD) simulations. In contrast to the earlier theoretical studies [33,34], our method uses the Newtonian equations motion to describe the lattice dynamics and calculates vibrational modes by following Boltzmann statistics, which is the high-temperature limit of Bose-Einstein statistics. This also allows for the modeling phonon dispersion at the room temperature by including the full anharmonicity of the atomic interactions (i.e. all orders of phonon-phonon interactions). Hence, this technique is a suitable theoretical modeling platform which produces temperature dependent vibrational and allows for a reasonable comparison to our angle-dependent Raman spectra measured at the room temperature.

2. Results and discussion

2.1. Twist angle characterization: TEM and Raman spectroscopy

Fig. 1(a–b) shows the scanning electron microscopy (SEM) and optical images of the single layer and bilayer graphene areas on the Cu foil and Si/SiO_2 respectively. The single layer graphene grains typically were 25–30 μm in size and overlapped with the neighbouring grains. The second layer of graphene nucleated near the centre of first grain and had an average size of ~5 μm. This is indicative that the centre of first (primary) layer acts as a preferential nucleation site for the growth of secondary layer. Growth parameters such as methane concentration, methane to hydrogen ratio and growth time were optimized to obtain the desired nucleation density of graphene grains and control the number of layers and grain size of each layer.

Fig. 2 shows the SAED obtained from different regions of the TEM grid with tBLG grains having different twist angles. The diffraction pattern obtained from the SLG region, (Fig. 2(a)), showed a hexagonal pattern, while that obtained from a tBLG (Fig. 2(b and c)) showed a diffraction pattern with two sets of hexagonal patterns rotated at a certain angle that is indicative of the relative twist angle θ between the stacked layers. This technique allows for determination of the twist angle with an accuracy of ±1°. Fig. 2(d) shows the population distribution of the different tBLG grains analysed in this study. Based on the population distribution, the stacked tBLG grains showed no preferred angular orientation and were randomly distributed across 0°–30°.

Fig. 3 shows the Raman spectra of different tBLG grains (having rotation angles $\theta = 5.8^\circ, 11.2^\circ, 12^\circ, 16^\circ, 24.7^\circ$ and 29.3°). The I_{2D}/I_G ratio, a parameter typically used to determine the number of layers, was >3 for single-layer graphene. For tBLG with smaller twist angles (<10°), the Raman spectra looks similar to that of few-layer graphene with $I_{2D}/I_G < 1$. While for tBLG with larger twist angles (>20°), the Raman spectra looks similar to that of single-layer graphene with the I_{2D}/I_G ratio >1. Additionally, the resonant enhancement of the G peak was observed for tBLG with $\theta_c = 12^\circ$. This agrees with the estimate of $\theta_c = \Delta k/K = 3aE_{laser}/\hbar v f 4\pi$ where a is the lattice parameter of graphene (2.46 Å), ħ is the reduced Planck's constant, and v_f is the Fermi velocity in monolayer graphene (10^6 m/s), E_{laser} is the energy of the excitation source [25].

The Raman spectra (G and 2D peaks) observed for tBLG with different twist angles was compared to other reports in literature [25,26] for validation of accuracy of twist angle measurement and the corresponding Raman signature. We analysed the peak widths (full width half maximum (FWHM)) and peak positions of the G and

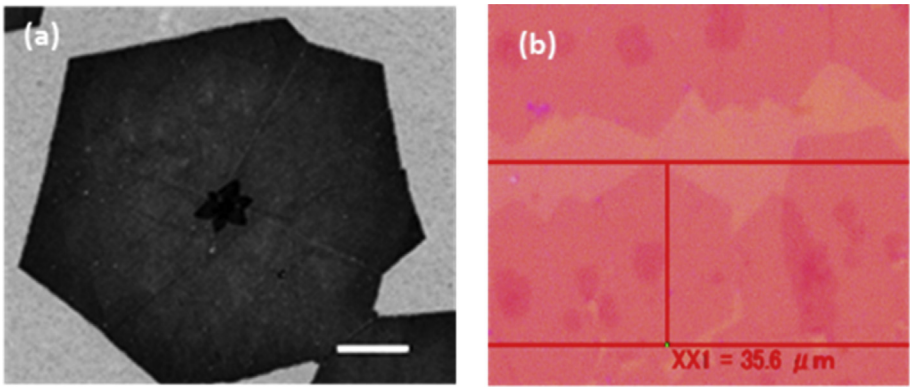

Fig. 1. **(a)** Scanning electron microscopy (SEM) images of graphene on Cu foil. The scale bar is 10 μm. **(b)** High magnification optical images of tBLG transferred on a Si/SiO_2 substrate. (A colour version of this figure can be viewed online.)

2D peaks as a function of twist angle θ. The detailed analysis is shown in the Supplementary Information. Briefly, for smaller twist angles, the G and 2D peak widths were broader compared to those of SLG. There was an increase around the resonant twist angle, $\theta_c = 12^\circ$. As θ increased above θ_c, the FWHM of the 2D peak monotonically decreased. The FWHM of the G peak had a plateau between 19° and 24.7°, and then decreased with a minimum at 30° that was close to the FWHM of SLG. The trends observed for intensity ratios and peak widths as a function of twist angle are indicative of layer decoupling with increasing twist angle and are similar to those reported in literature [25,26].

2.2. Low frequency modes: theory and experiment

To analyze the twist angle dependent evolution of the low-energy phonon modes, we performed molecular dynamics calculations of the phonon dispersion for commensurate rotation angles between 0° and 30°. Numerical details are provided in the Supplementary Information (Section 2). In tBLG, the ZO' (or ZA) modes, at frequency of ~95 cm^{-1}, correspond to inter-layer breathing modes and describe the coupling between the layers [30,38]. We identified these low-frequency ZO′ modes by analyzing both the direction and the magnitude of the out-of-plane displacements on each layer, as shown in the inset of Fig. 4(b). For all twist angles, the displacements of the identified ZO′ mode are purely out-of-plane as shown in the inset of Fig. 4(b) for 21.78° tBLG. For the other modes at Γ resulting from zone folding of the ZA branches, the displacements are a mix of in-plane and out-of-plane components, since these modes originate from low symmetry points in the original Brillouin zone. A detailed discussion and illustrations of the origins in the original Brillouin zone of the new modes appearing at Γ due to zone-folding are provided in Ref. [33]. The low-frequency ZO′ modes for all of the simulated tBLG systems are tabulated in Table 1.

Two exemplary low-frequency dispersions near Γ for twist angles 6.01° and 13.17° are shown in Fig. 4(a). The ZO′ mode at Γ is indicated by the red solid circle, and the frequencies corresponding to the acoustic branches and the zone-folded acoustic branches are indicated by the blue solid circles. Due to the large size of the

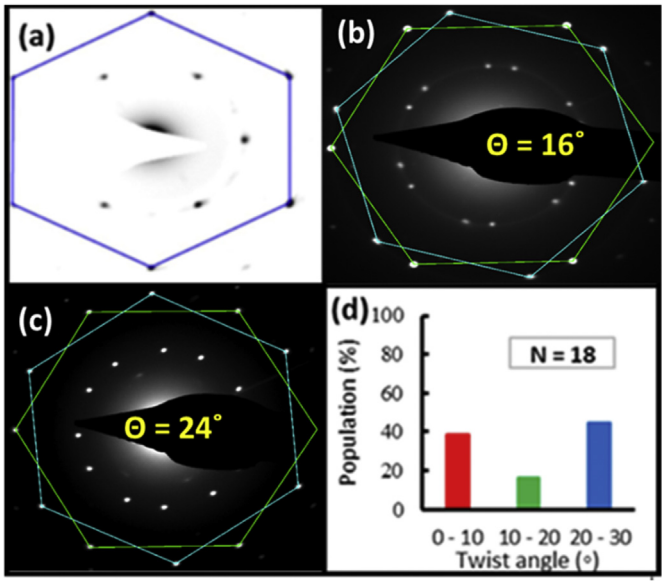

Fig. 2. Selected area electron diffraction patterns (SAED) at **(a)** SLG region showing a hexagonal pattern, **(b, c)** tBLG region exhibiting two sets of hexagonal patterns from the corresponding graphene layers rotated w.r.t. Each other at $\theta = 19^\circ$ and $\theta = 25^\circ$, respectively. **(d)** Histograms showing the population density of 18 different tBLG grains analysed using TEM. (A colour version of this figure can be viewed online.)

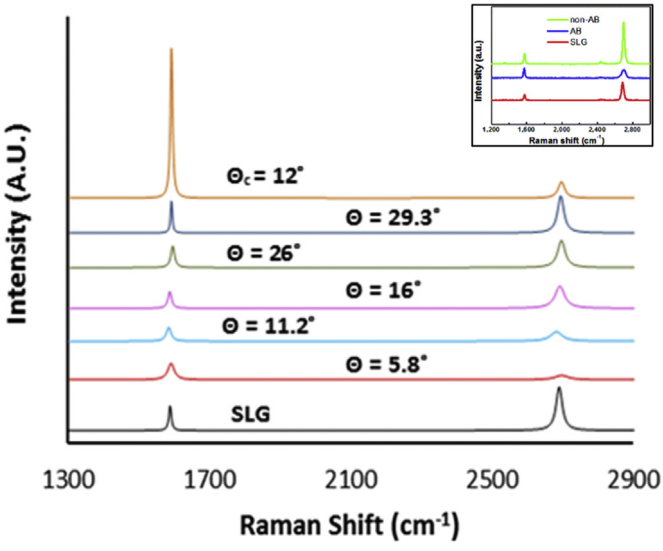

Fig. 3. Raman spectra of SLG and the different tBLG samples labelled with the corresponding twist angle determined using TEM. All Raman spectra were obtained using a 532 nm wavelength laser (2.33 eV). The experimentally observed peaks were fitted with a Lorentzian function and shifted vertically for clarity. The inset shows the comparison between the Raman spectra of SLG, AB-BLG and tBLG Raman spectra obtained from Ref. [22]. (A colour version of this figure can be viewed online.)

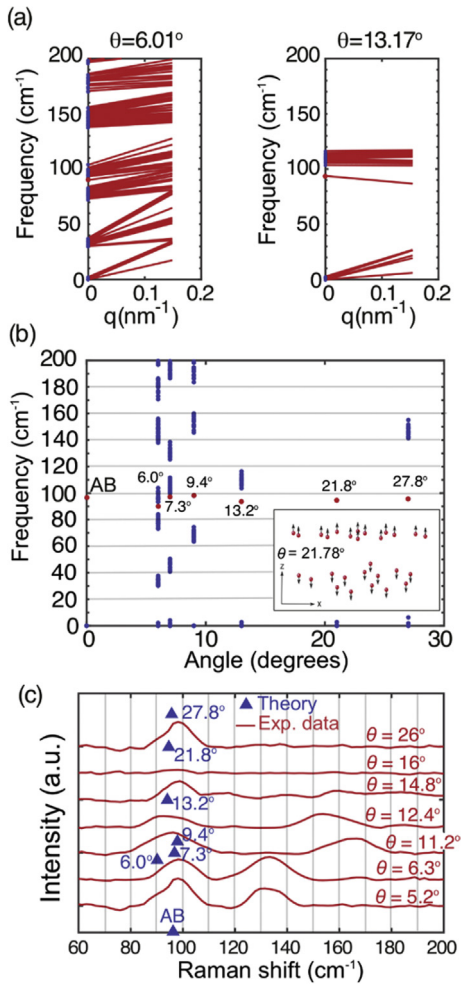

Fig. 4. (a) Calculated phonon dispersion near Γ with θ = 6.01°(left) and θ = 13.17°(right). The plots consist of only two q-points due to the large size of the supercells; **(b)** Phonon frequencies at Γ for different rotation angles. The red points are the ZO′ modes. The blue points are from the zone-folded acoustic modes. The inset shows atomic displacements for the low energy ZO′ mode at Γ with θ = 21.78°; and **(c)** Calculated ZO′ mode frequencies (blue triangles) plotted on top of the low-energy Raman spectrum from various experimentally observed twist angles in tBLG systems. The angles for the theoretical calculations are next to the data points. (A colour version of this figure can be viewed online.)

supercell, the plots consist of only two q points. Fig. 4(b) shows the same set of Γ-point frequencies for all calculated angles. For all angles, the ZO′ mode remains slightly set apart in frequency from the zone-folded ZA modes. The change in frequency of the ZO′ mode with respect to twist angle is relatively small except for the two angles shown in Fig. 4(a). The one relatively large frequency shift $\Delta f = -6.31$ cm^{-1} for the 6.0° rotation occurred when a band of ZA modes was folded back to Γ at the original ZO′ energy of ~95 cm^{-1}. Mode repulsion pushed the ZO′ mode down below the zone-folded band causing the large shift, as shown in Fig. 4(a,b). In the commensurate unit cells that we have simulated, the ZO′ mode and the manifolds of zone-folded ZA modes never intermix at Γ. They are never degenerate. The ZO′ and ZA branches do not cross near Γ, but push away from each other, in a manner similar to a mode anti-crossing in which a small coupling between modes results in mode repulsion. This mode repulsion causes a shift in the ZO′ mode when zone folding results in a degeneracy with a ZA mode.

A plot of the low-frequency experimental Raman spectrum for various measured twist angles is superimposed on the theoretically calculated ZO′ frequencies in Fig. 4(c). Note that the theoretically calculated angles corresponding to commensurate rotations do not exactly correspond to the experimentally measured samples, since only commensurate rotations can be simulated with periodic boundary conditions. The theoretical data points are placed close to the experimental curves with similar rotation angles. Qualitatively, a Raman peak does appear within a few cm^{-1} of the calculated ZO′ frequencies. Since, as can be seen from the last column of Table 1, the theoretical values shift by a few cm^{-1} for small changes in angle, and the theoretical angles are all one or more degrees different from the experimental angles, it is difficult to make a quantitative comparison. We can say that an experimental peak does occur in the expected frequency range of the ZO′ mode, that small shifts occur as a function of twist angle for both the experimental and theoretical values, and that the shifts are not monotonic functions of either the angle or the supercell lattice constant.

The next higher experimental Raman peak that appears for the smaller angle samples ($\theta \leq 14.8°$) in Fig. 4(c) is in the frequency range 120 cm^{-1} to 200 cm^{-1} where we theoretically observe new Γ-point modes resulting from the zone-folded ZA branch as shown in Fig. 4(b). The frequencies of these new Γ-point, zone-folded modes are more sensitive to the rotation angle than the frequencies of the ZO′ mode. Increasing the rotation angle by 1.3° from 6.0° to 7.3° causes a new band of modes to appear in the range between 120 and 140 cm^{-1}. Increasing the angle another 2° to 9.4° causes the band of modes to disappear. Thus, instead of shifts on the order of a few cm^{-1}, the shifts of these modes are on the order of 20 cm^{-1} or more. These large numerical shifts are consistent with the shifts seen in the experimental data of Fig. 4(c). For both the numerical calculation and the experimental data, these shifts are not monotonic functions of the angle, in contrast to the spectra plotted in Fig. 2(c) of Ref. [26] and Fig. 2(a) of Ref. [27]. We also observe Raman peaks at 130 cm^{-1} and 133 cm^{-1} for the low-angle rotations θ = 5.2° and θ = 6.3°, respectively, that are far from the resonant angle of 12°. To the best of our knowledge, these peaks in low-angle tBLG have not been observed previously.

3. Conclusions

The tBLG samples with twist angles varying from 0° to 30° were

Table 1
Evolution of the theoretically predicted frequency for the low-energy ZO′ mode as a function of twist angle ordered by supercell size. The change in frequency with respect to the AB structure is given in the far right column.

Twist angle (θ)	No. of atoms in the Supercell	Theoretically predicted low-frequency ZO′ modes (cm^{-1})	Change in frequency Δf (cm^{-1})
AB	4	96.44	0.0
21.78°	28	94.56	−1.88
27.79°	54	95.66	−0.78
13.17°	76	93.76	−2.68
9.43°	148	97.97	1.53
7.34°	244	96.94	0.50
6°	364	90.13	−6.31

synthesized using chemical vapor deposition and suspended on a TEM grid. To study the twist angle dependent vibrational properties, the Raman signature was obtained for the various tBLG grains with different twist angles. For each tBLG grain, the relative twist angle between the graphene layers was determined using selected area electron diffraction (SAED). The Raman G and 2D peak shape and frequencies followed the same trends as reported in earlier studies. Raman peaks in the range 120 cm^{-1} to 200 cm^{-1} were observed for the lower angle samples and the results are consistent with the previous observations. Unlike previous results, strong peaks of ~130 cm^{-1} were observed for the two lowest angles of 5.2° and 6.3° that were far from the resonant angle of 12°. Both numerically and experimentally, angle-dependent small shifts of a few cm^{-1} were observed in the ZO′ mode, and this mode was also experimentally observed at angles of 26°, 6.3°, and 5.2° that were far from the resonant angle. The calculated phonon spectra of the commensurate rotation angles and the zone-folding picture provide insight into the general positions and variations of the Raman peaks of the tBLG structures.

Acknowledgements

The work at UC River side was supported, in part, by the National Science Foundation grant no. 1307671 and by W. Ruel Johnson Chair in Environmental Engineering. This work was supported by grants of computer time from the DOD High Performance Computing Modernization Program at the U.S. Air Force Research Laboratory and U.S. Army Engineer Research and Development Center DoD Supercomputing Resource Centers.

Appendix A. Supplementary data

Supplementary data related to this article can be found at http://dx.doi.org/10.1016/j.carbon.2017.07.064.

References

[1] A.K. Geim, K.S. Novoselov, The rise of graphene, Nat. Mater 6 (3) (2007) 183–191.
[2] A.A. Balandin, S. Ghosh, W. Bao, I. Calizo, D. Teweldebrhan, F. Miao, C.N. Lau, Superior thermal conductivity of single-layer graphene, Nano Lett. 8 (3) (2008) 902–907.
[3] C. Lee, X. Wei, J.W. Kysar, J. Hone, Measurement of the elastic properties and intrinsic strength of monolayer graphene, Science 321 (5887) (2008) 385–388.
[4] K.S. Novoselov, A.K. Geim, S.V. Morozov, D. Jiang, Y. Zhang, S.V. Dubonos, I.V. Grigorieva, A.A. Firsov, Electric field effect in atomically thin carbon films, Science 306 (5696) (2004) 666–669.
[5] Z. Yan, G. Liu, J.M. Khan, A.A. Balandin, Graphene quilts for thermal management of high-power GaN transistors, Nat. Commun. 3 (2012) 827.
[6] L. Gomez De Arco, Y. Zhang, C.W. Schlenker, K. Ryu, M.E. Thompson, C. Zhou, Continuous, highly flexible, and transparent graphene films by chemical vapor deposition for organic photovoltaics, ACS Nano 4 (5) (2010) 2865–2873.
[7] L. Liao, Y.C. Lin, M. Bao, R. Cheng, J. Bai, Y. Liu, Y. Qu, K.L. Wang, Y. Huang, X. Duan, High-speed graphene transistors with a self-aligned nanowire gate, Nature 467 (7313) (2010) 305–308.
[8] S. Shallcross, S. Sharma, E. Kandelaki, O.A. Pankratov, Electronic structure of turbostratic graphene, Phys. Rev. B 81 (16) (2010), 165105.
[9] R. Bistritzer, A.H. MacDonald, Moiré butterflies in twisted bilayer graphene, Phys. Rev. B 84 (3) (2011), 035440.
[10] R. Bistritzer, A.H. MacDonald, Moiré bands in twisted double-layer graphene, Proc. Natl. Acad. Sci. 108 (30) (2011) 12233–12237.
[11] P. Moon, M. Koshino, Energy spectrum and quantum Hall effect in twisted bilayer graphene, Phys. Rev. B 85 (19) (2012), 195458.
[12] Z.F. Wang, F. Liu, M.Y. Chou, Fractal Landau-level spectra in twisted bilayer graphene, Nano Lett. 12 (7) (2012) 3833–3838.
[13] T. Ohta, A. Bostwick, T. Seyller, K. Horn, E. Rotenberg, Controlling the electronic structure of bilayer graphene, Science 313 (5789) (2006) 951–954.
[14] K.S. Novoselov, E. McCann, S.V. Morozov, V.I. Fal'ko, M.I. Katsnelson, U. Zeitler, D. Jiang, F. Schedin, A.K. Geim, Unconventional quantum Hall effect and Berry's phase of 2π in bilayer graphene, Nat. Phys. 2 (3) (2006) 177–180.
[15] J.B. Oostinga, H.B. Heersche, X. Liu, A.F. Morpurgo, L.M. Vandersypen, Gate-induced insulating state in bilayer graphene devices, Nat. Mater 7 (2) (2008) 151–157.
[16] B. Partoens, F.M. Peeters, From graphene to graphite: electronic structure around the K point, Phys. Rev. B 74 (7) (2006), 075404.
[17] E.V. Castro, K.S. Novoselov, S.V. Morozov, N.M. Peres, J.L. Dos Santos, J. Nilsson, F. Guinea, A.K. Geim, A.C. Neto, Biased bilayer graphene: semiconductor with a gap tunable by the electric field effect, Phys. Rev. Lett. 99 (21) (2007), 216802.
[18] J.L. Dos Santos, N.M. Peres, A.C. Neto, Graphene bilayer with a twist: electronic structure, Phys. Rev. Lett. 99 (25) (2007), 256802.
[19] A. Luican, G. Li, A. Reina, J. Kong, R.R. Nair, K.S. Novoselov, A.K. Geim, E.Y. Andrei, Single-layer behavior and its breakdown in twisted graphene layers, Phys. Rev. Lett. 106 (12) (2011), 126802.
[20] J.L. Dos Santos, N.M. Peres, A.C. Neto, Continuum model of the twisted graphene bilayer, Phys. Rev. B 86 (15) (2012), 155449.
[21] K.M. Habib, S.S. Sylvia, S. Ge, M. Neupane, R.K. Lake, The coherent interlayer resistance of a single, rotated interface between two stacks of AB graphite, Appl. Phys. Lett. 103 (24) (2013), 243114.
[22] H. Li, H. Ying, X. Chen, D.L. Nika, A.I. Cocemasov, W. Cai, A.A. Balandin, S. Chen, Thermal conductivity of twisted bilayer graphene, Nanoscale 6 (22) (2014) 13402–13408.
[23] V. Carozo, C.M. Almeida, E.H. Ferreira, L.G. Cançado, C.A. Achete, A. Jorio, Raman signature of graphene superlattices, Nano Lett. 11 (11) (2011) 4527–4534.
[24] R.W. Havener, H. Zhuang, L. Brown, R.G. Hennig, J. Park, Angle-resolved Raman imaging of interlayer rotations and interactions in twisted bilayer graphene, Nano Lett. 12 (6) (2012) 3162–3167.
[25] K. Kim, S. Coh, L.Z. Tan, W. Regan, J.M. Yuk, E. Chatterjee, M.F. Crommie, M.L. Cohen, S.G. Louie, A. Zettl, Raman spectroscopy study of rotated double-layer graphene: misorientation-angle dependence of electronic structure, Phys. Rev. Lett. 108 (24) (2012) 246103.
[26] R. He, T.F. Chung, C. Delaney, C. Keiser, L.A. Jauregui, P.M. Shand, C.C. Chancey, Y. Wang, J. Bao, Y.P. Chen, Observation of low energy Raman modes in twisted bilayer graphene, Nano Lett. 13 (8) (2013) 3594–3601.
[27] J. Campos-Delgado, L.G. Cançado, C.A. Achete, A. Jorio, J.P. Raskin, Raman scattering study of the phonon dispersion in twisted bilayer graphene, Nano Res. 6 (4) (2013) 269–274.
[28] C.H. Lui, L.M. Malard, S. Kim, G. Lantz, F.E. Laverge, R. Saito, T.F. Heinz, Observation of layer-breathing mode vibrations in few-layer graphene through combination Raman scattering, Nano Lett. 12 (11) (2012) 5539–5544.
[29] S. Coh, L.Z. Tan, S.G. Louie, M.L. Cohen, Theory of the Raman spectrum of rotated double-layer graphene, Phys. Rev. B 88 (16) (2013), 165431.
[30] J.A. Yan, W.Y. Ruan, M.Y. Chou, Phonon dispersions and vibrational properties of monolayer, bilayer, and trilayer graphene: density-functional perturbation theory, Phys. Rev. B 77 (12) (2008), 125401.
[31] N. Mounet, N. Marzari, First-principles determination of the structural, vibrational and thermodynamic properties of diamond, graphite, and derivatives, Phys. Rev. B 71 (20) (2005), 205214.
[32] M. Droth, G. Burkard, Acoustic phonons and spin relaxation in graphene nanoribbons, Phys. Rev. B 84 (15) (2011), 155404.
[33] A.I. Cocemasov, D.L. Nika, A.A. Balandin, Phonons in twisted bilayer graphene, Phys. Rev. B 88 (3) (2013), 035428.
[34] J.W. Jiang, B.S. Wang, T. Rabczuk, Acoustic and breathing phonon modes in bilayer graphene with Moiré patterns, Appl. Phys. Lett. 101 (2) (2012).
[35] I. Calizo, A.A. Balandin, W. Bao, F. Miao, C.N. Lau, Temperature dependence of the Raman spectra of graphene and graphene multilayers, Nano Lett. 7 (9) (2007) 2645–2649.
[36] C.C. Lu, Y.C. Lin, Z. Liu, C.H. Yeh, K. Suenaga, P.W. Chiu, Twisting bilayer graphene superlattices, ACS Nano 7 (3) (2013) 2587–2594.
[37] W. Regan, N. Alem, B. Alemán, B. Geng, Maserati L. Girit Ç, F. Wang, M. Crommie, A. Zettl, A direct transfer of layer-area graphene, Appl. Phys. Lett. 96 (11) (2010), 113102.
[38] L.M. Malard, J. Nilsson, D.C. Elias, J.C. Brant, F. Plentz, E.S. Alves, A.C. Neto, M.A. Pimenta, Probing the electronic structure of bilayer graphene by Raman scattering, Phys. Rev. B 76 (20) (2007), 201401.